PNAS RESEARCH ARTICLE | APPLIED PHYSICAL SCIENCES

Gas plasma–oxidized sodium chloride acts via hydrogen peroxide in a model of peritoneal carcinomatosis

Lea Miebach[a,b,1], Eric Freund[a,b,1], Ramona Clemen[a], Stephan Kersting[b], Lars-Ivo Partecke[b,c], and Sander Bekeschus[a,2]

Edited by David Weitz, Harvard University, Cambridge, MA; received January 13, 2022; accepted June 13, 2022

Gas plasma technology generates reactive oxygen and nitrogen species (ROS/RNS), inducing lethal oxidative damage in tumor cells. The transfer of gas plasma–derived ROS/RNS into liquids has been proposed as an innovative anti-cancer strategy targeting peritoneal carcinomatosis (PC). However, the mechanism of action is under debate. To this end, we compared gas plasma–oxidized medical-grade sodium chloride (oxNaCl) with a concentration-matched control (cmc) of NaCl enriched with equivalent concentrations of H_2O_2 and NO_3^- in several cell lines and models of PC. Strikingly, oxNaCl and cmc performed equally well in oxidation and cytotoxic activity in tumor cells in two-dimensional cultures, three-dimensional (3D) tumor spheroids, vascularized 3D tumors grown on chicken-embryo chorioallantoic membranes, and a syngeneic PC mouse model in vivo. Given the importance of immunotherapies in oncology today, we focused on immunological consequences of the treatment. Again, to a similar extent, oxNaCl and cmc increased tumor cell immunogenicity and enhanced uptake by and maturation of peripheral blood monocyte–derived dendritic cells together with an inflammatory secretion profile. Furthermore, NanoString gene expression profiling revealed immune system processes and unfolded protein response-related pathways as being linked to the observed anti-tumor effects for both oxNaCl and cmc. In conclusion, gas plasma–generated oxNaCl and cmc showed equal therapeutic efficacy in our PC-related models. In light of the many promising anti-cancer studies of gas plasma–oxidized liquids and the convenient production of corresponding cmcs in large quantities as needed in clinics, our findings may spur research lines based on low-dose oxidants in peritoneal cancer therapy.

ICD | immunogenicity | ROS | plasma medicine | calreticulin

Significance

Reactive oxygen/nitrogen species (ROS/RNS) were long considered unwanted byproducts that cells have to neutralize. However, the field of redox biology discovered that ROS/RNS are often produced by intent and used as signaling molecules. Recently, novel technologies such as gas plasma have aimed at generating vast levels of ROS for therapeutic purposes. One of these purposes is loading liquids with ROS to target cancer that has spread in the abdomen. Here, we unraveled the mechanism of these liquids as hydrogen peroxide. This finding is dramatic as it allows transferring findings from plasma technology to redox biology. Moreover, low-dose hydrogen peroxide is easy to produce and is known in clinics. Our findings may open a chapter of redox intervention in cancer management.

Maintaining cellular redox homeostasis is crucial for cellular survival. Thus, targeting of the intracellular redox state has become a significant research field in clinical oncology in recent years (1). Due to specific biochemical alterations, tumor cells are particularly vulnerable to oxidation-induced lethal damage by exogenous agents (2). This concept is exploited by reactive oxygen and nitrogen species (ROS/RNS)–generating therapies, including photodynamic therapy (3) and other emerging technologies such as medical gas plasmas. Nonetheless, until now the application of available plasma devices has been confined to locally restricted, superficially growing, or ulcerating (in palliative settings) tumors and their precancerous stages.

The administration of gas plasma–oxidized liquids can be considered for internal and largely disseminated neoplasms such as peritoneal carcinomatosis. While direct plasma applications drive especially short-lived ROS/RNS chemistries that can be enhanced at a specified site (4), plasma-oxidized liquids act through long-lived ROS/RNS emerging from secondary reactions of gas-phase species (5). Previously, some studies aimed to clarify the biological relevance of the emerging species and found that hydrogen peroxide (H_2O_2) plays a central role (6). Despite being interesting from a mechanistic perspective, the opportunity to mimic gas plasma–derived ROS/RNS chemistry would consequently question the need for complex gas plasma systems in the oxidized liquid generation process. Moreover, generation of the larger volumes required for clinical application is not feasible with current gas plasma sources and would require the costly process of medical device or even drug approval. Consequently, such a liquid must be substantially superior to the sum of ingredients that could be generated at a fraction of the cost. Since the overall idea is the future integration of ROS-induced tumor cell death in oncological treatment concepts, the application of manually enriched fluids would not only be a significant step toward clinical approval but would also facilitate their routine application as a therapeutic strategy. Based on clinical routines, the only feasible liquids for such an approach—independent of being ROS/RNS enriched by a gas plasma process or via chemical addition—are approved medical products and not cell culture media.

Author affiliations: [a]ZIK plasmatis, Leibniz Institute for Plasma Science and Technology, 17489 Greifswald, Germany; [b]Department of General, Visceral, Thoracic, and Vascular Surgery, Greifswald University Medical Center, 17475 Greifswald, Germany; and [c]Department of General, Visceral, and Thoracic Surgery, Helios Clinic Schleswig, 24837 Schleswig, Germany

Author contributions: L.M., E.F., S.K., L.-I.P., and S.B. designed research; L.M., E.F., and R.C. performed research; L.M., E.F., R.C., S.K., L.-I.P., and S.B. contributed new reagents/analytic tools; L.M., E.F., and S.B. analyzed data; and L.M. and S.B. wrote the paper.

The authors declare no competing interest.

This article is a PNAS Direct Submission.

[1]L.M. and E.F. contributed equally to this work.

[2]To whom correspondence may be addressed. Email: sander.bekeschus@inp-greifswald.de.

This article contains supporting information online at http://www.pnas.org/lookup/suppl/doi:10.1073/pnas.2200708119/-/DCSupplemental.

Published July 28, 2022.

In that view, the present study comprises a thorough screening of anti-tumor effects induced by gas plasma–oxidized saline (oxNaCl) solutions in a head-to-head comparison with a solution containing chemically added equimolar amounts of the main long-lived species H_2O_2 and nitrate produced by the gas plasma process (referred to as concentration-matched control [cmc]). Treatment efficacy was evaluated in in vitro and in vivo cancer cell models of peritoneal carcinomatosis with a specific focus on immunological consequences of the treatment. Profiling of differential gene expression patterns combined with gene set enrichment analysis served to identify globally initiated expression pathways among all tumor cell lines.

Materials and Methods

Generation of oxNaCl and a cmc. Sufficient amounts of oxNaCl solutions were generated by exposing 50 mL 0.9% saline (Braun) in a 250-mL glass beaker to medical gas plasma for 30 min and 90 min. Gas plasma treatment was performed using the atmospheric pressure plasma jet kINPen MED (neoplas MED) operated with five standard liters per minute of argon gas (99.999% purity; Air Liquide). The device is approved as a medical product class IIa in Europe. The distance between jet nozzle and liquid phase was 15 mm (Fig. 1*A*). Immediately after gas plasma treatment, evaporated volume was replaced with predetermined amounts of double-distilled water to reestablish iso-osmolarity. oxNaCl solutions were stored in aliquots of 1.5 mL at −20 °C for subsequent experiments. Based on the quantification of H_2O_2 and nitrate (NO_3^-) generated by 30 min of gas plasma exposure of sodium chloride solution, untreated sodium chloride was spiked with equimolar concentrations of chemical grade H_2O_2 and NO_3^- to mimic oxNaCl chemically. The solution was termed cmc and stored similarly to oxNaCl. NO_2^- was not added due to its low concentration at this treatment time and its absence after one freeze-thaw cycle.

Animal Experiments. Experimental procedures were reviewed and approved by the local authority Landesamt für Landwirtschaft, Lebensmittelsicherheit und Fischerei and the ethical committee of Mecklenburg-Vorpommern (approval number: 7221.3-1-048/18-1). Peritoneal carcinomatosis was induced in Balb/C mice by intraperitoneal (i.p.) injection of 4×10^5 murine (syngeneic) colon carcinoma cells (CT26). Starting on day 4, mice received an i.p. injection of 250 µL of NaCl, oxNaCl, or cmc solutions every 2 d. On day 13, mice were killed, and tumor burden was assessed by tumor weight after careful excision. Tumor nodules were embedded in freezing medium (Tissue-Tek O.C.T.; Sakura Europe) following cryopreservation in liquid nitrogen for subsequent tissue staining.

Additional materials and methods are provided in the *SI Appendix*, to which the reader is also referred for supplemental results and analyses.

Results

Profiling Reactive Species oxNaCl Solutions. Gas plasma–oxidized liquids favor a broad range of anti-tumor effects triggered by oxidative distress in response to excessive ROS/RNS exposure. Sufficient amounts of oxNaCl were generated and immediately stored at −20 °C for subsequent experiments (Fig. 1*A*). Upon gas plasma treatment, unbuffered oxNaCl solutions experienced a slight decline in pH (*SI Appendix*, Fig. S1*A*). Given their low stability, highly reactive gas-phase species quickly deteriorate in bulk liquids (*SI Appendix*, Fig. S1*B–D*) and generate a few stable ROS/RNS in secondary reactions. Quantification of H_2O_2 revealed a pronounced increase corresponding to 200 µM after 90 min of gas plasma treatment (Fig. 1*B*). In addition, NO_3^- (Fig. 1*C*) and its reduced precursor NO_2^- (*SI Appendix*, Fig. S1*E*), but not HOCl (*SI Appendix*, Fig. S1*F*), were generated in the current gas regimen. Predetermined concentrations of H_2O_2 (80 µM) and NO_3^- (8 µM) generated with 30 min of gas plasma exposure served to prepare a cmc containing 80 µM of H_2O_2 and 8 µM of NO_3^-, which was investigated head-to-head with oxNaCl in subsequent experiments. Both solutions were prepared on the same day, stored in the same way, and used for experiments in a similar fashion. To confirm the equivalency of oxNaCl and cmc, ROS/RNS profiles were investigated after one freeze-thaw cycle and differed only slightly between both types of liquid (*SI Appendix*, Table S1).

oxNaCl and cmc Equally Promote Lethal Oxidative Damage in Two-Dimensional (2D) and Three-Dimensional (3D) Tumor Models. Cells exhibit a variety of mechanisms to preserve cellular redox homeostasis and eliminate or respond to ROS/RNS immediately, such as glutathione (GSH), which dimerizes to GSSG after oxidation. Upon exposure to oxNaCl and cmc (Fig. 1*D*), a significant intracellular GSSG increase was observed (Fig. 1*E*) in two out of three cell lines investigated (Fig. 1*F*, *I–III*), which was rescued by addition of H_2O_2-scavenging (*SI Appendix*, Fig. S2*A*) catalase (*SI Appendix*, Fig. S2*B*, *I–III*). However, there was no significant difference in GSSG increase between oxNaCl and cmc in any cell type. Upon excessive ROS/RNS exposure, cellular redox capacities potentially failed to secure intracellular molecules from irreversible damage, resulting in reduced metabolic activity (*SI Appendix*, Fig. S3, *I–III*) and induction of cell death signaling pathways. Exogenous (gas plasma–derived) ROS can trigger endogenous ROS generation (*SI Appendix*, Fig. S4*A–C*), further amplifying antitumor effects. Flow cytometric analysis (Fig. 1*G*) revealed a tumor-toxic rather than tumor-static action of both oxNaCl and cmc solutions (Fig. 1*H*, *I–III*) that was abrogated by prior catalase addition (*SI Appendix*, Fig. S2*C*, *I–III*). Next, the anticancer efficacy of these solutions was investigated in 3D tumor spheroids that drive tumor cell differentiation throughout the different spatial zones, providing a physiologically more complex and relevant model for the investigation of therapeutic approaches. 3D tumorspheres formed from cultured tumor cells were achieved successfully in HT-29 and SKOV3 but not Panc-01 cells (Fig. 1*I*). Monitoring of spheroid volume and fluorescence intensity of a cell death dye (sytox blue) over 72 h revealed a marked decline in HT-29 (Fig. 1*J*). However, testing in SKOV3 spheroids was hampered by the sodium chloride addition alone, which already decelerated spheroid growth and induced cytotoxic effects (Fig. 1*K*). No significant difference between oxNaCl and cmc was observed in either cell line.

oxNaCl and cmc Equally Promote Proapoptotic Signaling Paralleled by Up-Regulation of Ecto-Calreticulin (CRT). Toxicity in response to oxNaCl and cmc solutions was characterized by caspase 3 and 7 activation, a hallmark for proapoptotic signaling (Fig. 2*A*). Apart from oxNaCl showing higher toxicity than cmc in SKOV3 cells, the response amplitude was similar for oxNaCl and cmc in the other two cell types investigated. Caspase 3 and 7 activation (*SI Appendix*, Fig. S2*D*) was drastically reduced in the presence of catalase in Panc-01 and SKOV3 cells (*SI Appendix*, Fig. S2*E*). While apoptosis is often described as "silent" cell death, since apoptotic cells do not initiate uncontrolled inflammatory reactions, this form of cell death can still be immunogenic (7). Cells undergoing immunogenic cell death (ICD) show enhanced surface expression of so-called damage-associated molecular patterns (DAMPs). Surface translocation of the endoplasmic reticulum (ER) CRT (Fig. 2*B*), one of the most prominent ICD-associated molecules, was increased in response to treatment with oxNaCl and cmc solutions to a similar extent in two cell lines, while no increase was observed for either agent in HT-29 cells (Fig. 2*C*, *I–III*). Again, the addition of catalase abolished the ability of oxNaCl to enhance CRT expression in dying cancer cells (*SI Appendix*, Fig. S2*F*).

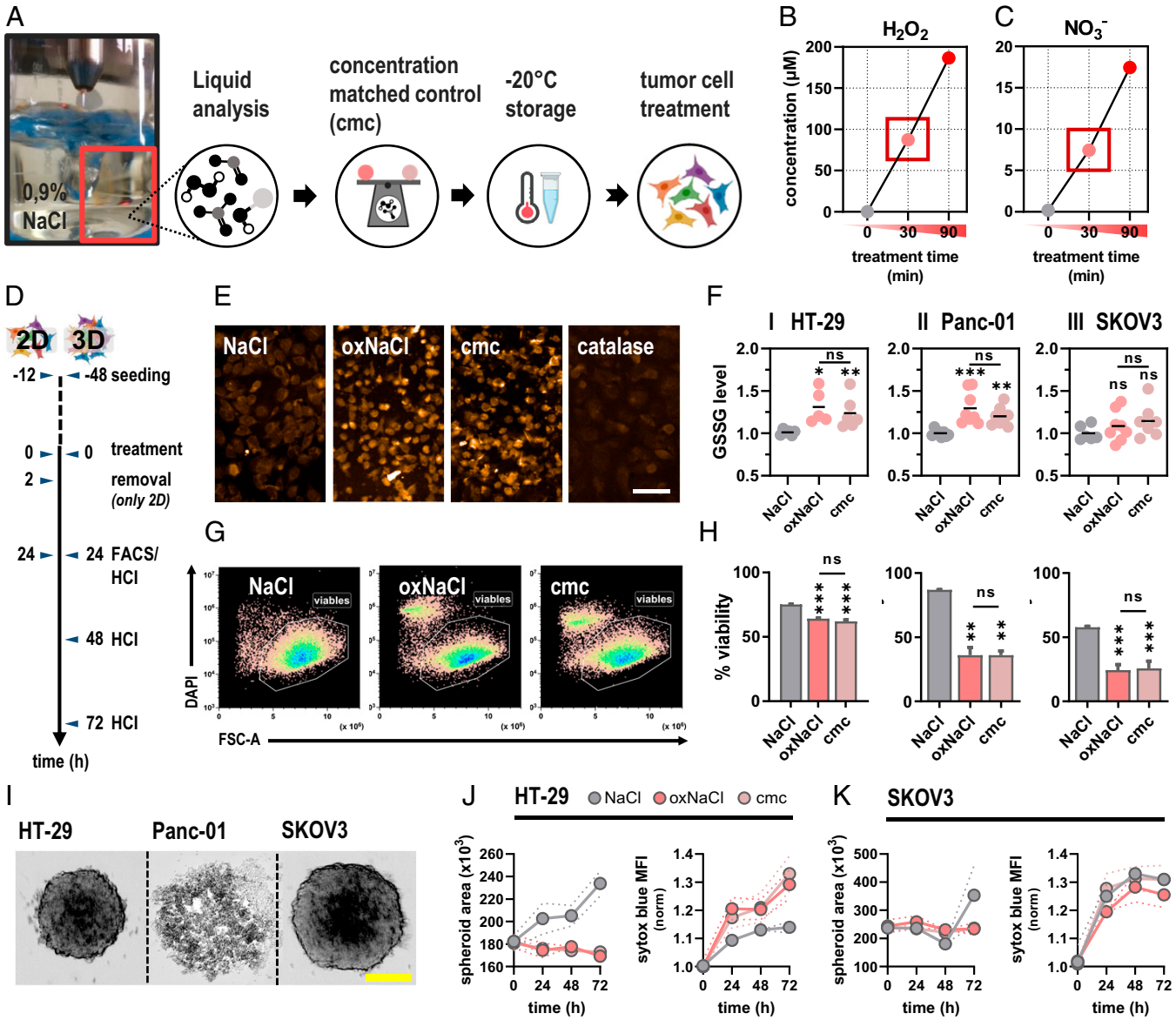

Fig. 1. Gas plasma treatment of sodium chloride (oxNaCl) deposits mainly H_2O_2 and NO_3^-, which was mimicked in a cmc to elicit lethal oxidative stress in tumor cells. (*A*) Schematic overview of liquid preparation and storage for subsequent experiments. (*B* and *C*) Quantification of H_2O_2 (*B*) and NO_3^- (*C*). (*D*) Schematic overview of experimental treatment procedures in 2D and 3D cell culture models. (*E*) Representative fluorescence microscopy images of oxidized glutathione (GSSG) in cells exposed to either oxNaCl or cmc. (Scale bar, 20 µm.) (*F*) GSSG quantification. (*G*) Representative flow cytometry dot plots of cells. (*H*) Quantification of viable HT-29 (I), Panc-01 (II), and SKOV3 (III). (*I*) Representative brightfield images of HT-29, Panc-01, and SKOV3 tumor spheroids. (Scale bar, 200 µm.) (*J* and *K*) Kinetic evaluation of spheroid growth in HT-29 (*J*) and SKOV3 (*K*) tumor spheroids and nucleic acid–staining sytox blue. Graphs show mean ± SEM (SEM). Statistical analysis was performed using ANOVA. (*$P < 0.05$, **$P < 0.01$, ***$P < 0.001$; ns, nonsignificant). FACS, fluorescence activated cell sorting; HCl, high content imaging; DAPI, 4′,6-Diamidino-2-phenylindol; MFI, mean fluorescence intensity.

oxNaCl and cmc Equally Promote Tumor Cell Uptake by Dendritic Cells (DCs) and an Enhanced Inflammatory Profile. Enhanced expression of ecto-CRT, as observed in vitro following exposure to oxidized saline solutions, can act as an "eat me" signal for antigen-presenting cells such as DCs. In order to validate whether exposure to oxNaCl and cmc solutions induces bona fide ICD, resulting in increased cytokine release and interaction between immature DCs (iDCs) and pretreated tumor cells, coculture experiments were performed (Fig. 2*D*). Assessment of surface markers on cocultured DCs revealed a significant increase of molecules associated with DC maturation and activation, such as CD11c, CD86, and HLA-DR (Fig. 2*E*, *I–III*). The phagocytic activity of DCs toward tumor cells was evaluated by fluorescently labeling both cell populations. Uptake of tumor material (DiD^+) was detected by quantification of $CD11c^+/DiD^+$ cells (Fig. 2*F*) and was significantly enhanced when tumor cells had been exposed to oxidized saline solutions before (Fig. 2*G*, *I–III*), without significant differences between oxNaCl and cmc in most cases. The cocultures were accompanied by several changes in the cytokine- and chemokine-release profiles (Fig. 2*H*). oxNaCl conditions elicited moderately increased levels of interleukin (IL)-10 and tumor necrosis factor (TNF)α and a more pronounced increase in CC-chemokine ligand (CCL)4, IL-6, and interferon γ-induced protein (IP)-10. These mediators were also increased with cmc conditions that strongly induced interferon (IFN)-γ, transforming growth factor (TGF)-β1, and IL-1β release in addition. While absolute fold-changes in concentrations differed for some of these targets, their overall regulation (i.e., increase or decrease or similar levels) was mostly consistent between oxNaCl and cmc, as underlined by the principal component analysis (PCA) (Fig. 2*I*).

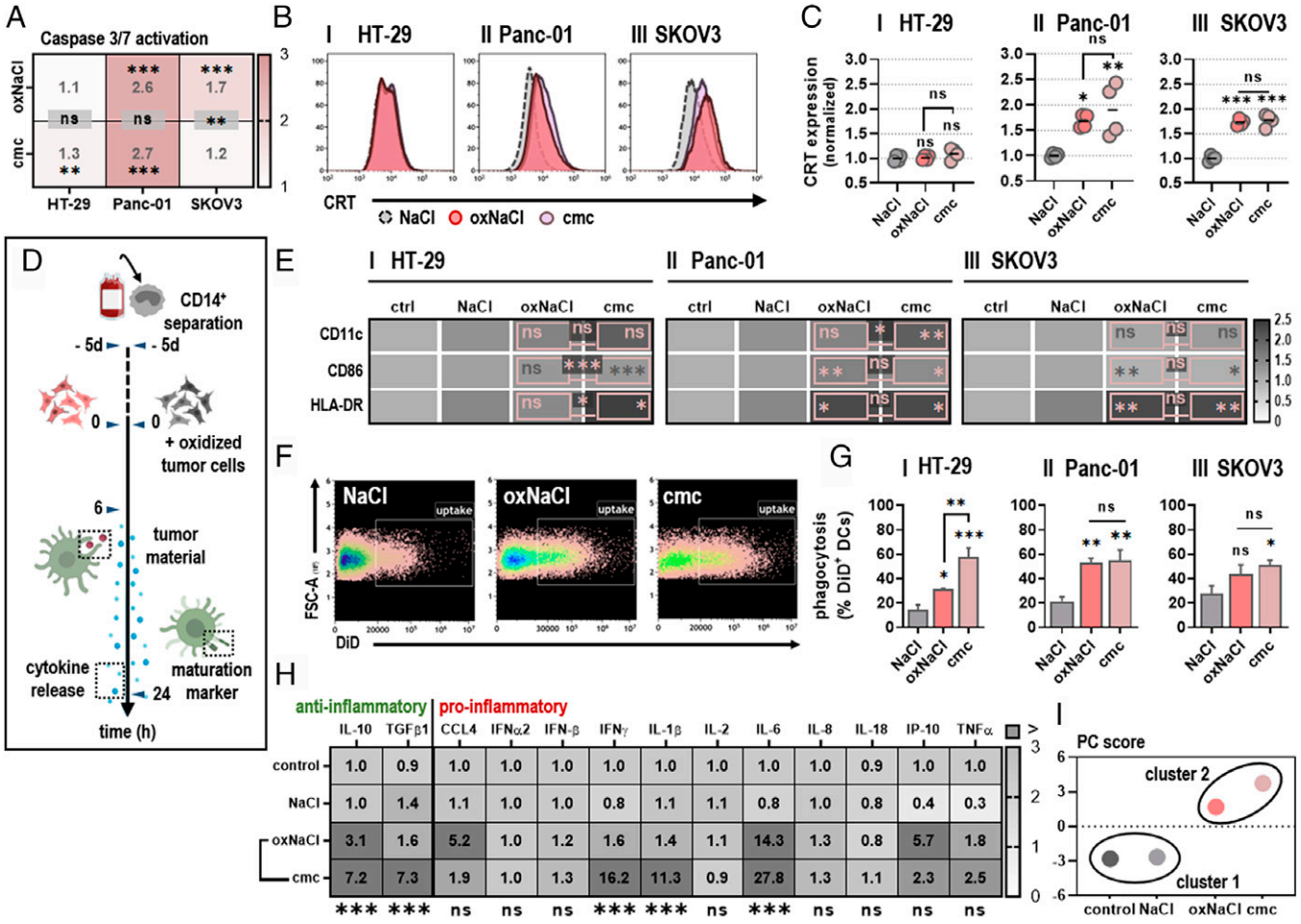

Fig. 2. oxNaCl and cmc equally promote tumor cell uptake by DCs and an enhanced inflammatory profile. (*A*) Quantification of apoptotic HT-29 (I), Panc-01 (II), and SKOV3 (III) cells normalized to NaCl. (*B*) Representative flow cytometry intensity histograms of CRT surface expression of viable cells. (*C*) CRT MFI quantification and normalization for HT-29 (I), Panc-01 (II), and SKOV3 (III) cells. (*D*) Schematic overview of experimental treatment procedure for coculture experiments. (*E*) Quantification of DC maturation markers cocultured with tumor cells cultured in medium (control [ctrl]), NaCl, oxNaCl, or cmc and normalized to controls. (*F*) Representative flow cytometry dot plots of CD11c+/DiD+ DCs. (*G*) Quantification of phagocytosis of HT-29 (I), Panc-01 (II), SKOV3 (III) tumor cells previously exposed to liquids as labeled. (*H*) Chemokine and cytokine profiles in supernatants of DCs cocultured with tumor cells cultured in medium (control), NaCl, oxNaCl, or cmc and normalized to controls. (*I*) Principal component (PC) score calculated from maturation marker and cytokine release profiles of DCs cocultured with tumor cells cultured in medium (control), NaCl, oxNaCl, and cmc. Bar graphs show mean + (SEM). Heat maps show median. Statistical analysis was performed using one-way ANOVA. (*$P < 0.05$, **$P < 0.01$, ***$P < 0.001$; ns, nonsignificant). MFI, mean fluorescence intensity.

oxNaCl and cmc Induced Comparable Changes in Gene Expression Profiling. Functional gene expression analysis of HT-29, Panc-01, and SKOV3 cells after exposure to oxidized saline solutions was performed after 4 h of incubation using NanoString technology. PCA of z-scored differential gene expression showed overall similar responses between oxNaCl- and cmc-treated tumor cells (Fig. 3*A*), with differences observed between both regimens in resistant HT-29 cells as indicated by a markedly different principal component 1. SKOV3 cells, which were already shown to succumb to untreated NaCl (Fig. 1*K*), displayed dissimilar expression patterns upon exposure to NaCl compared to HT-29 and Panc-01 cells. With this heterogeneity in mind, we subsequently subjected genes differentially regulated in at least two cell lines in response to oxNaCl or cmc treatment to further analysis. In the overlapping regions in the Venn diagrams (Fig. 3*B*), 26 genes were found to be regulated in at least two cell lines upon oxNaCl and/or cmc treatment, contributing to a pool of 21 genes. Comparison of median gene expression patterns indicated overall similar responses after treatment with oxNaCl solutions compared to cmc, with only slight differences between them (Fig. 3*C*). Interestingly, protein network analysis had already displayed a strong interconnection between corresponding proteins (Fig. 3*D*). Subsequent pathway enrichment analysis revealed immune system, IL signaling, response to oxygen-containing compounds, p53 pathway, and inflammatory response processes as top categories of these genes (Fig. 3*E*). Notably, process category priority was the same between oxNaCl and cmc exposure regimens.

Finally, the relative reduction in viability in all cell lines after both treatments was correlated with expression patterns of differentially regulated genes among all cell lines. Spearman correlation revealed that the expression level of x-box binding protein 1 (XBP-1), a transcription factor involved in unfolded protein response (UPR) signaling upon ER stress, correlated strongly and significantly with cytotoxicity in response to oxNaCl or cmc solutions (Fig. 3*F*). XBP-1 is a target of activating transcription factor (ATF) 6 and is activated upon splicing by inositol-requiring enzyme 1 (IRE1). While gene expression levels of the latter were increased in two out of three cell lines investigated (*SI Appendix*, Fig. S6*A*), nuclear translocation of ATF6 (*SI Appendix*, Fig. S6*C*) was observed upon exposure to oxNaCl and cmc (*SI Appendix*, Fig. S6*D*). Increased protein expression levels of the spliced variant of XBP-1 (Fig. 3*G*) were found consistently (*SI Appendix*, Fig. S6*B*).

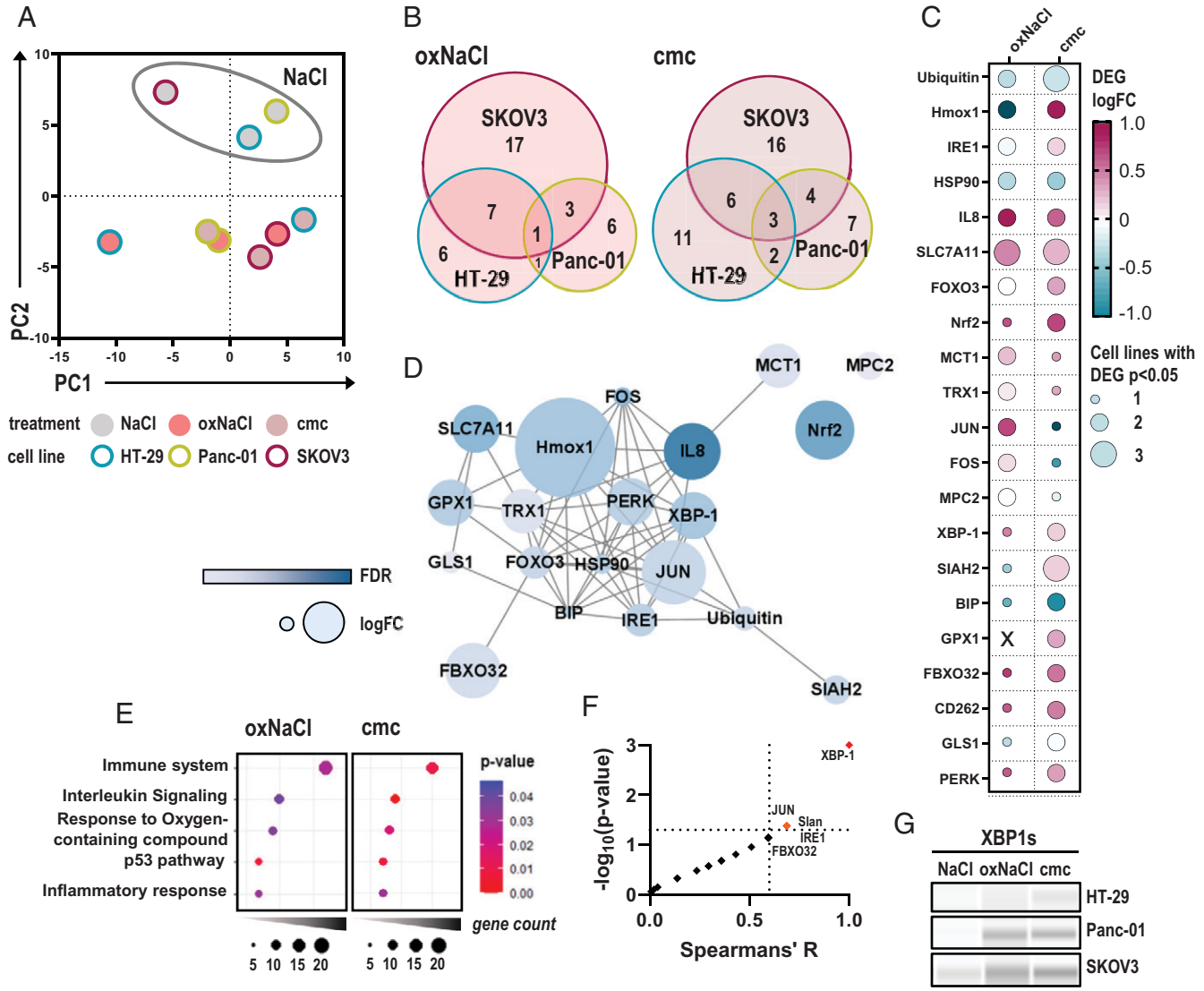

Fig. 3. oxNaCl and cmc induce comparable changes in gene expression profiling. (*A*) PCA of z-scored gene expression patterns in HT-29, Panc-01, and SKOV3 tumor cells 4 h after exposure to respective solutions. (*B*) Venn diagrams. (*C*) Median log fold-changes (logFCs) of 21 differentially expressed genes (DEGs) in at least two cell lines and one treatment regimen (oxNaCl or cmc). (*D*) String interaction network of corresponding proteins. (*E*) Pathway enrichment dot plots of gene ontology (GO) terms after exposure to oxNaCl (*Left*) and cmc solutions (*Right*). (*F*) Spearman correlation of % viability reduction against log fold-changes (logFC) of DEGs. (*G*) Representative Western blot images of XBP-1s expression in HT-29, Panc-01, and SKOV3 cell lines 6 h after exposure to NaCl, oxNaCl, or cmc. FDR, false discovery rate.

oxNaCl and cmc Equally Reduce Tumor Burden In Ovo and a Syngeneic Model of Peritoneal Carcinomatosis In Vivo. To increase the level of tumor model complexity, the tumor–chorioallantoic membrane (CAM) assay was employed next. In this model, tumors become vascularized at later stages of culture and form an extracellular matrix. After tumors were grown for 4 d on the CAM, a single exposure to NaCl, oxNaCl, and cmc was carried out (Fig. 4*A*). SKOV3 tumors were used as a model due to their low responsiveness in the spheroid model. Yet, neither oxNaCl nor cmc was able to reduce SKOV3 growth significantly (*SI Appendix*, Fig. S5). However, in vivo tumors are often infiltrated with immune cells, and we had observed phagocytosis of tumor cells in our previous experiments (Fig. 2*G*). Accordingly, we further increased the complexity of this model by coculturing both human tumor cells and peripheral blood monocyte–derived DCs on the CAM in ovo. Interestingly, significant declines (Fig. 4*B*) were observed for both oxNaCl and cmc that, again, were not significantly different from each other (Fig. 4*C*).

Up to this point, the in vitro and in ovo data suggested a similar performance for oxNaCl and its corresponding cmc in terms of cytotoxic and inflammatory effects. Despite the advanced nature of these models, in vivo vertebrate models are closest when it comes to mimicking the patient situation. As plasma-treated liquids were proposed for the treatment of peritoneal carcinomatosis, we therefore used syngeneic CT26 cells engrafted into the peritoneal cavity of Balb/c mice to test the liquids' efficacy in reducing tumor burden. By intent, we avoided using the human cancer cell lines investigated above, as peritoneal carcinomatosis xenograft models have not been established for these cell types. In addition, we wanted to avoid using mice with a hampered immune system, as the dramatic progress of antitumor (and antiviral) immunology and immunotherapy of the past decade readily exemplifies the need to include the effects of immune cells on the disease and therapy in question. To this end, mice suffering from peritoneal carcinomatosis received an i.p. injection of oxidized saline solutions every 2 d in five treatment cycles (Fig. 4*D*). Excised tumor nodules were cryo-embedded for

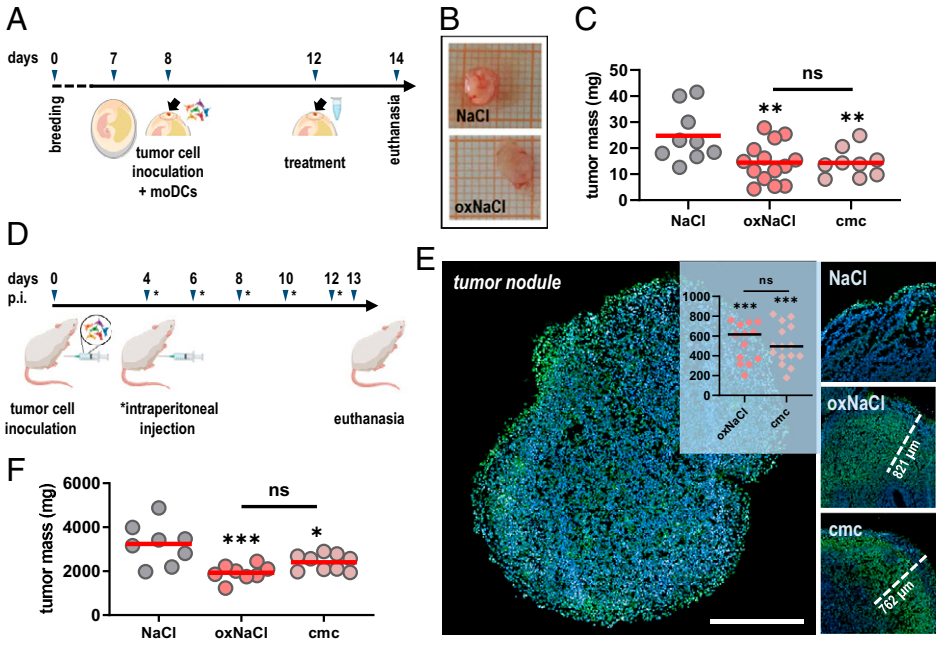

Fig. 4. oxNaCl and cmc equally reduce tumor burden in ovo and in a syngeneic model of peritoneal carcinomatosis in vivo. (*A*) Schematic overview of experimental treatment procedure in ovo. (*B*) Representative images of excised in ovo tumors. (*C*) Assessment of tumor weight of in ovo tumor cell–DC coculture tumors. (*D*) Schematic overview of experimental treatment procedure in vivo. (*E*) Representative images of TUNEL-stained tumor nodules indicative for apoptosis with representative distance marks of penetration depths and quantification thereof (*Insert*: *y* axis shows penetration depth with regard to dead cell regions reaching within the tissues expressed in micrometers). (*F*) Tumor weight of excised peritoneal tumor nodules. Graphs show mean. Statistical analysis was performed using one-way ANOVA (*$P < 0.05$, **$P < 0.01$, ***$P < 0.001$; ns, nonsignificant). (Scale bar, 1 mm.) moDC, monocyte-derived DCs.

subsequent terminal deoxynucleotidyl transferase-mediated dUTP nick end labeling (TUNEL) staining of apoptotic cells. Marked apoptotic regions were identified in peritoneal tumors repeatedly exposed to oxNaCl and cmc alike, penetrating deep into the nodules to cause the apoptosis (Fig. 4*E*). Strikingly, peritoneal lavage with both oxNaCl and cmc successfully reduced tumor burden in tumor-bearing mice without significant differences between the treatments (Fig. 4*F*).

Notably, treatment with both types of liquids was safe. First, a certain degree of selectivity was found, as liquid exposure did not increase GSSG levels in nonmalignant HaCaT keratinocytes (*SI Appendix*, Fig. S10*A*) compared to the tumor cells (Fig. 1*F*). Second, administration of both liquids did not induce animal weight loss, indicative of overall compatible reception by the mice (*SI Appendix*, Fig. S10*B*). Third, application of both liquids in the hen's egg test (HET)-CAM model (*SI Appendix*, Fig. S10*C*), was excellently tolerated compared to highly concentrated 2% H_2O_2 routinely used in dentistry worldwide (*SI Appendix*, Fig. S10*C*), as evaluated by irritation potential scoring (*SI Appendix*, Fig. S10*E* and *F*).

H_2O_2 Correlates with a Proimmunogenic Marker Expression Profile. These data provided evidence that oxNaCl acts via H_2O_2 to elicit ICD in cancer cells. However, cell-heterogenic responses were observed, as HT-29 failed to up-regulate CRT completely at the H_2O_2 concentrations initially tested. In this regard, we wondered whether H_2O_2 could promote up-regulation of immune-related and immunogenic surface markers in a dose-dependent fashion, switching regulated cell death from nonimmunogenic apoptosis to bona fide ICD (Fig. 5*A*). To this extent, surface expression of the myeloid checkpoint CD47, proimmunogenic CRT, high mobility group box 1 (HMGB1), heat shock protein (HSP) 70, and the tumor necrosis factor receptors (TNFRs) I and II were assessed using flow cytometry 6 h after exposure to different H_2O_2 concentrations (Fig. 5*B*). HT-29 and Panc-01 cells showed similar responses with increasing concentrations of H_2O_2 (Fig. 5*C*). Higher H_2O_2 concentrations elicited CRT exposure in HT-29 cells, indicating that the cmc regimen tested initially (Fig. 2*B*) operated below the critical point to trigger CRT up-regulation. Nonetheless, relative increases in HT-29 cells were lower than in Panc-01 cells (Fig. 5*D*). Pearson correlation underlined a strong correlation between H_2O_2 dosage and immune-related and immunogenic marker profiles (Fig. 5*E*). Separate analyses of surface marker expression profiles in viable and dead cells underlined comparable alterations for increasingly dosed H_2O_2 (*SI Appendix*, Fig. S7) and oxNaCl (*SI Appendix*, Fig. S8). Dose–response relationships correlated to surprisingly high degrees for most markers investigated in both types of exposures (*SI Appendix*, Table S2).

Discussion

Gas plasma–oxidized liquids have contributed considerably to understanding of the biomedical relevance of ROS/RNS in oncological treatment concepts, such as lavage in peritoneal carcinomatosis patients. However, the mechanism of action is under debate, while from a redox chemistry point of view, only long-lived oxidants such as H_2O_2 and NO_3^- are stable enough to persist in gas plasma–treated liquids that can be stored for clinical application. To this end, we compared gas plasma–oxidized medical-grade sodium chloride (oxNaCl) against a cmc of NaCl enriched with equimolar concentrations of H_2O_2 and NO_3^- in several cell lines and models of peritoneal carcinomatosis.

As early as 2013, it was reported that for an argon plasma jet, the toxicity of treated cell culture media was mainly dependent on H_2O_2 (8). Accordingly, several reports added H_2O_2 as controls in their experiments, albeit only a few used H_2O_2 concentrations exactly matched to those generated by the gas plasma device in the liquid exposed. For instance, Ma and colleagues (9) found that their cmc mimicked the amplitude of

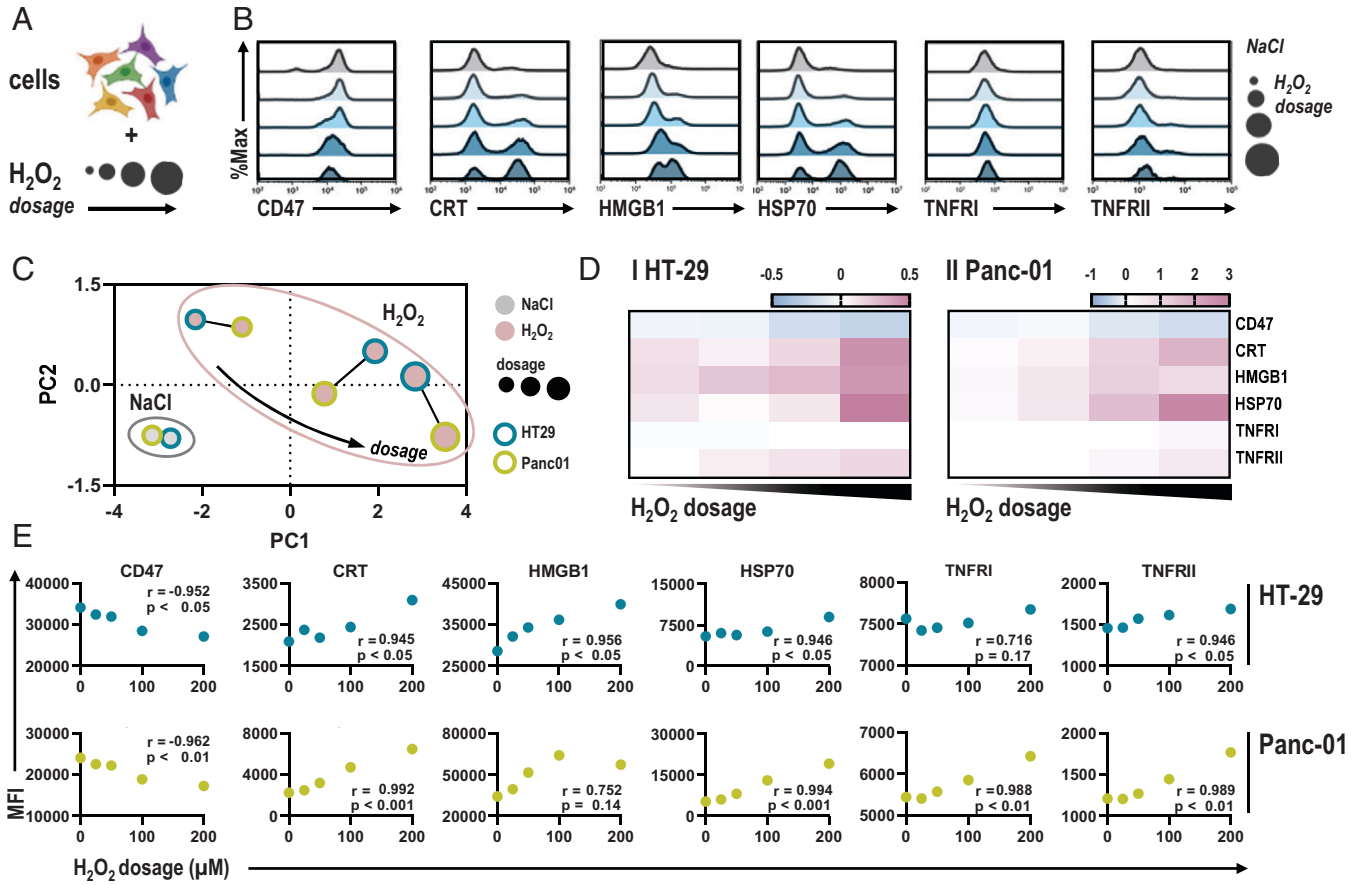

Fig. 5. H_2O_2 dosage correlates with immune-related and immunogenic surface marker expression profiles. (*A*) Schematic overview of experimental procedure. (*B*) Representative flow cytometry intensity histograms of CD47, CRT, HMGB1, HSP 70, and TNFR I and II. (*C*) PCA of z-scored marker expression profiles in HT-29 and Panc-01 cells. (*D*) Quantification of marker expression normalized to NaCl in HT-29 and Panc-01 cells. (*E*) Pearson correlation of marker MFI and H_2O_2 dosage. Heat map shows median. Graphs show mean. MFI, mean fluorescence intensity.

apoptosis only partially; however, they had used direct gas plasma treatment as a comparator. They also suggested ozone as a toxic contributor, but this oxidant has low solubility in liquids, as indicated by Henry's constant (10). Strikingly, they found that the H_2O_2 degrading enzyme catalase abolished gas plasma–mediated cytotoxicity fully. Likewise, plasma-treated saline (PTS) cytotoxicity in 3D tumor spheroids was blocked if catalase was present prior to treatment (11). The same finding was made in B16 melanoma cells (12), skin fibroblasts (13), and gas plasma–treated medium in lung cancer cells (14) and peripheral blood mononuclear cells (15). In the present work, similar results were obtained concerning GSSG levels, induction of cell death signaling, and CRT exposure if catalase was added to NaCl prior to gas plasma treatment and exposure of cells to oxNaCl (*SI Appendix*, Fig. S2). The role of NO_3^- in our study was likely negligible, as it was recently shown that H_2O_2 and NO_3^- do not show combined cytotoxicity (16). NO_2^- was detected only in low amounts and was neglected with regard to its diminished stability when assayed in thawed liquid samples. Although these reports suggest a prominent role of H_2O_2 in the toxic effects of PTS, our study comprehensively compared a cmc to a PTS (oxNaCl) across several biological model systems using a liquid that is a medical product (i.e., for clinical application).

An extensive range of cancer cell types have been found to succumb to PTS-induced toxicity in vitro and partially also in vivo, including glioblastoma (17), melanoma (12), osteosarcoma (18), ovarian carcinoma (19), lung cancer (20), pancreatic cancer (21), and squamous cell carcinoma (22). Attributing ROS-induced toxicity to a certain cell death modality is complicated not only by heterogeneous and cell type–specific death responses but also in consideration of the pleiotropic roles that ROS exhibit in a multitude of physiological signaling pathways per se. Many reports have found apoptosis to be the central cell death mechanism induced by PTS (23), in line with caspase 3 and 7 activation in our study. However, studies have recently suggested other cell death pathways such as necroptosis (24) and autophagy (25), which were not investigated in our study.

In recent years, enhancement of the immune system has represented a breakthrough in cancer treatment (26). One approach is to trigger a proimmunogenic phenotype in dying cancer cells. CRT translocation is linked to ICD (27). At initially tested concentrations of oxidizing salines, Panc-01 and SKOV3 but not HT-29 cells showed signs of ICD as indicated by increased expression of ecto-CRT (28). Intriguingly, evaluation of mutational profiles based on official cell line sequencing databases (CCLE, COSMIC) identified a stop-gained variant in *CASP8* [c.1342C > T (p.Q448*)] in HT-29, affecting the peptidase region of encoded caspase 8. Successful up-regulation of CRT requires an apoptotic module essentially dependent on the former, as shown by almost complete abolition of CRT exposure in $casp8^{-/-}$ cells (28). In addition, the reduced ability of HT-29 cells to expose ecto-CRT has been reported before (29). In our study, higher H_2O_2 concentrations elicited CRT exposure in HT-29 cells to a low but notable extent, indicating that the initial oxNaCl and cmc solutions tested (Fig. 2*B*) were too low in

H_2O_2 concentration to elicit ICD in HT-29 cells. On dying cells, CRT acts as an eat me signal for innate immune cells such as DCs. Binding to its receptor low density lipoprotein related receptor-1 (CD91) on phagocytic cells leads to subsequent maturation of iDCs and enhanced phagocytosis of tumor material (30). Surprisingly, we observed an up-regulation of maturation markers and elevated phagocytosis in DCs cocultured with oxNaCl- or cmc-treated tumor cells, with largely similar absolute uptake levels across the three cell lines. Due to the complex nature of ICD, molecules other than CRT might have contributed to HT-29 cell phagocytosis that was overall similar to that of SKOV3 despite the higher CRT levels in the latter. However, baseline SKOV3 phagocytosis was already increased compared to that of HT-29 and Panc-01 cells. An array of phagocytosis checkpoint molecules have recently come into focus, which may explain the apparent discrepancy between CRT expression and phagocytosis (31). Chemokine and cytokine analysis revealed an increase of TNFα, IL-1β, IL-6, CCL4, IP-10, and IFN-γ. TNFα and IL-1β are known to induce apoptosis and contribute to cytotoxic effects in cancer treatment (32, 33). CCL4 and IP-10 act as strong chemoattractants, resulting in increased leukocyte infiltration into the tumor microenvironment (34, 35). However, we also observed a simultaneous increase in immunosuppressive TGF-β1 and IL-10 levels (36). Overall, oxNaCl- and cmc-treated tumor cells induced similar effects in DCs. Our findings are in line with data from Van Loenhout and colleagues (37), who observed an immunogenic phenotype of pancreatic cancer cells exposed to gas plasma–treated phosphate-buffered saline (PBS), which led to increased phagocytosis and expression of maturation markers. Tomić and colleagues (38) had recently shown that gas plasma–treated cell culture medium inactivated melanoma cells in an immunogenic fashion, which led to elevated uptake and maturation of DCs and subsequently dampened tumor-supportive T helper 2 cell responses.

The three cell lines investigated in this study did not always show congruent results. Tumor cell fate is governed by cell-intrinsic properties that are closely engaged with the extrinsic influence of the surrounding environment. Suggestions have been made regarding factors that influence 1) the ability of ROS to enter the cell, 2) cell maintenance of cellular redox hemostasis, and 3) intracellular baseline ROS level. For instance, some members of the aquaporin membrane water channel family can also transport H_2O_2, and it has been suggested that their increased expression would render cells more sensitive to plasma-derived ROS in view of facilitated ROS entry. Similar implications have been given to membrane cholesterol content that heavily impacts the stiffness of the lipid bilayer. Also, cell lines displaying an altered redox metabolism (e.g., if having constitutive excess to cysteine for GSH biosynthesis) have been shown to be more resistant to gas plasma exposure (39). Intriguingly, correlation analysis across 35 cell lines revealed a strong correlation between expression levels of cell cycle–related genes and sensitivity toward H_2O_2 exposure (40), alongside reports of higher oxidative stress resistance of cells in the G0/G1 phase. SKOV3 cells, which showed neither increased consumption in glutathione nor increased toxicity after exposure to oxNaCl and cmc in spheroids or in ovo, were found with the highest proportion of cells in the G0/G1 phase. However, substantial toxicity toward untreated NaCl per se markedly limited related conclusions in vitro. Moreover, G1/G2 ratios were equal between HT-29 cells, identified as the most resistant cell line, and Panc-01 cells, by contrast the most sensitive among all cell lines (*SI Appendix*, Fig. S9*A* and *B*). Among the top target genes negatively correlating with resistance to H_2O_2 (40), *TUBB*, encoding for tubulin beta chain, was expressed five times higher in sensitive Panc-01 than in resistant HT-29 cells (*SI Appendix*, Fig. S9*C*). This makes tubulin a candidate for investigating oxidative stress resistance in more detail in the future.

Profiling of differential gene expression patterns served to identify globally initiated signaling pathways and compare responses to the respective liquids. XBP-1, a transcription factor involved in signaling cascades of the UPR, was identified as correlating highly and significantly with cytotoxicity in response to oxidized saline solutions. UPR signaling aims to restore vital ER-related protein folding capacity upon exposure to endo- or exogenous stressors that cause ER quality mechanisms to fail (41). Often referred to as a double-edged sword in cancer therapy, UPR signaling promotes adaptive responses, cell survival, and proliferation under modest ER stress conditions (42). By contrast, if the amount of oxidative stress exceeds a certain level, proapoptotic downstream factors, including IRE1, ATF4, C/EBP homologous protein (CHOP), and Nrf2, are expressed (43–45). Concerning XBP-1, disparate mechanisms are reported. XBP-1 messenger RNA is activated by unconventional splicing (spliced x-box binding protein [XBP-1s]) downstream of IRE1α signaling. Exclusive initiation of this signaling pathway has been linked to poor outcomes in patients suffering from various types of cancer. However, in the case of simultaneous PERK activation, XBP-1s contributes to CHOP-mediated apoptosis signaling (46), which coincides with the observed in vitro and in vivo antitumor effects observed in our study. Moreover, XBP-1 splicing together with ATF6 nuclear translocation, both observed upon exposure to oxNaCl and cmc (*SI Appendix*, Fig. S6), have been mechanistically linked to DAMP release and thereby employed as surrogate biomarkers for the detection of ICD (47).

From a translational perspective, the choice of liquid to be oxidized is critically important. Cell culture media, especially if they contain nonstandardized fetal calf serum, are not medical products applicable to patients. In addition, their complex formulation discourages such use, and we are not aware of any efforts to facilitate the approval of cell culture medium for clinical application. Such regulatory aspects are central to motivating translational research of PTS from a clinician's perspective. Moreover, different plasma-treated cell culture media and ingredients have been used for cancer cell treatment, each with different antioxidant capacities scavenging gas plasma–derived ROS/RNS. For instance, IMDM essentially loses its ability to induce cytotoxic PTS effects compared to RPMI (48). Pyruvate, a component of many culture media, was shown to scavenge PTS effects as well (18, 49). However, gas plasma–treated PBS (not a medical product for clinical application) was significantly more toxic in tumor and nontumor cells than its Dulbecco's modified Eagle's medium counterpart (50).

In our work using medical-grade sodium chloride, we identified cmc as being similarly effective compared to gas plasma–produced oxNaCl. While these findings may discourage use of gas plasma technology in this specific setup and treatment indication, this opens novel therapeutic avenues for patients suffering from peritoneal carcinomatosis. Low-dose oxidant-enriched liquids, such as NaCl spiked with H_2O_2 in the micromolar range, possess a strong translational capacity, with both agents already being medical products. Numerous studies have shown the lack of side effects of PTS in vivo (51–53), suggesting similar tolerability of cmc in such applications, which is supported by findings in the present work (*SI Appendix*, Fig. S10). In addition, micromolar-ranged H_2O_2 was also shown to combine with chemotherapeutic drugs to enhance cytotoxicity (54). In addition, the field of gas plasma research still struggles with

devices capable of generating several liters of treated liquids as needed in clinics [e.g., during hyperthermic i.p. chemotherapy employed in patients suffering from peritoneal carcinomatosis (55)]. From a regulatory perspective, the generation, packaging, storability, and quality control of H_2O_2-enriched liquids are more straightforward than use of large-volume plasma discharge reactors. Notwithstanding this, it would be fascinating to unravel unique plasma features in treated liquids that mediate biological effects without being reproducible by long-lived oxidant chemistry. One such approach was made by Tanaka et al. (56), showing that plasma-induced lactate modifications in Ringer's lactate, a medical product used in clinics, confers antitumor activity. Although appropriate controls were missing for ruling out an effect based on long-lived gas plasma–derived products that are also reproducible by chemical means, it is evident that short-lived reactive species—making gas plasmas unique—mediate oxidative modifications in biomolecules such as amino acids, which was not reproducible with long-lived oxidants (57–60). However, for some amino acids spiked into PBS prior to gas plasma exposure, cytotoxicity of such "storage" capacity could not be shown (50).

In conclusion, our study outlines the potential of oxidant-enriched liquids, independent of the oxidant's source, to be included in therapeutic strategies in clinical oncology and extends current knowledge on their mechanistic action. As cellular responses to oxNaCl and cmc solutions were strikingly comparable, we suggest that cmc solutions would be a feasible alternative to gas plasma–oxidized liquids in clinical application. In light of the many promising anticancer studies of gas plasma–treated liquids and the convenient production of corresponding cmcs at large quantities as needed in clinics, our findings may spur research lines based on low-dose non–plasma-derived oxidants in peritoneal cancer therapy (*SI Appendix*, Fig. S11).

Data Availability. All study data are included in the article and/or *SI Appendix*.

ACKNOWLEDGMENTS. Technical support by Felix Niessner, Fariba Saadati, and Anke Schmidt is gratefully acknowledged. Funding was received from the German Federal Ministry of Education and Research (Grant Nos. 03Z22DN11 and 03Z22Di1 to S.B.) and the Gerhard-Domagk-Foundation (Greifswald, Germany) scholarship to L.M.

1. D. Trachootham, J. Alexandre, P. Huang, Targeting cancer cells by ROS-mediated mechanisms: A radical therapeutic approach? *Nat. Rev. Drug Discov.* **8**, 579–591 (2009).
2. L. Tong, C. C. Chuang, S. Wu, L. Zuo, Reactive oxygen species in redox cancer therapy. *Cancer Lett.* **367**, 18–25 (2015).
3. D. E. Dolmans, D. Fukumura, R. K. Jain, Photodynamic therapy for cancer. *Nat. Rev. Cancer* **3**, 380–387 (2003).
4. L. Miebach, E. Freund, R. Clemen, K. D. Weltmann, H. R. Metelmann, T. von Woedtke *et al.*, Conductivity augments ROS and RNS delivery and tumor toxicity of an argon plasma jet. *Free Radic. Biol. Med.* **180**, 210–219 (2022).
5. P. J. Bruggeman *et al.*, Plasma-liquid interactions: A review and roadmap. *Plasma Sources Sci. Technol.* **25**, 053002 (2016).
6. G. Bauer, Targeting protective catalase of tumor cells with cold atmospheric plasma- activated medium (PAM). *Anticancer Agents Med. Chem.* **18**, 784–804 (2018).
7. L. Galluzzi, A. Buqué, O. Kepp, L. Zitvogel, G. Kroemer, Immunogenic cell death in cancer and infectious disease. *Nat. Rev. Immunol.* **17**, 97–111 (2017).
8. J. Winter *et al.*, Feed gas humidity: A vital parameter affecting a cold atmospheric-pressure plasma jet and plasma-treated human skin cells. *J. Phys. D Appl. Phys.* **46**, 295401 (2013).
9. J. Ma *et al.*, Contribution of hydrogen peroxide to non-thermal atmospheric pressure plasma induced A549 lung cancer cell damage. *Plasma Process. Polym.* **14**, 1600162 (2017).
10. J. Ferre-Aracil, S. C. Cardona, J. Navarro-Laboulais, Determination and validation of Henry's constant for ozone in phosphate buffers using different analytical methodologies. *Ozone Sci. Eng.* **37**, 106–118 (2014).
11. F. Judee *et al.*, Short and long time effects of low temperature plasma activated media on 3D multicellular tumor spheroids. *Sci. Rep.* **6**, 1 (2016).
12. J.-R. Liu *et al.*, Low-temperature plasma induced melanoma apoptosis by triggering a p53/PIGs/caspase-dependent pathway *in vivo* and *in vitro*. *J. Phys. D Appl. Phys.* **52**, 315204 (2019).
13. M. Horiba, T. Kamiya, H. Hara, T. Adachi, Cytoprotective effects of mild plasma-activated medium against oxidative stress in human skin fibroblasts. *Sci. Rep.* **7**, 42208 (2017).
14. T. Matsuzaki, A. Kano, T. Kamiya, H. Hara, T. Adachi, Enhanced ability of plasma-activated lactated Ringer's solution to induce A549 cell injury. *Arch. Biochem. Biophys.* **656**, 19–30 (2018).
15. S. Bekeschus *et al.*, Hydrogen peroxide: A central player in physical plasma-induced oxidative stress in human blood cells. *Free Radic. Res.* **48**, 542–549 (2014).
16. M. Ma *et al.*, Differences in cytotoxicity induced by cold atmospheric plasma and exogenous RONS solutions on human keratinocytes and melanoma cells. *IEEE Trans. Radiat. Plasma Med. Sci.* **5**, 835–842 (2021).
17. H. Tanaka *et al.*, Plasma-activated medium selectively kills glioblastoma brain tumor cells by down-regulating a survival signaling molecule, AKT kinase. *Plasma Med.* **1**, 265–277 (2011).
18. J. Tornin *et al.*, Pyruvate plays a main role in the antitumoral selectivity of cold atmospheric plasma in osteosarcoma. *Sci. Rep.* **9**, 10681 (2019).
19. K. Nakamura *et al.*, Novel intraperitoneal treatment with non-thermal plasma-activated medium inhibits metastatic potential of ovarian cancer cells. *Sci. Rep.* **7**, 6085 (2017).
20. Y. Li *et al.*, Low-temperature plasma-jet-activated medium inhibited tumorigenesis of lung adenocarcinoma in a 3D in vitro culture model. *Plasma Process. Polym.* **18**, 2100049 (2021).
21. N. Hattori *et al.*, Effectiveness of plasma treatment on pancreatic cancer cells. *Int. J. Oncol.* **47**, 1655–1662 (2015).
22. C. M. Lee, Y. I. Jeong, M. S. Kook, B. H. Kim, Combinatorial effect of cold atmosphere plasma (cap) and the anticancer drug cisplatin on oral squamous cell cancer therapy. *Int. J. Mol. Sci.* **21**, 7646 (2020).
23. Y. J. Cheng *et al.*, Plasma-activated medium as adjuvant therapy for lung cancer with malignant pleural effusion. *Sci. Rep.* **10**, 18154 (2020).
24. T. Ando *et al.*, Combined anticancer effect of plasma-activated infusion and salinomycin by targeting autophagy and mitochondrial morphology. *Front. Oncol.* **11**, 593127 (2021).
25. N. Yoshikawa *et al.*, Plasma-activated medium promotes autophagic cell death along with alteration of the mTOR pathway. *Sci. Rep.* **10**, 1614 (2020).
26. F. S. Hodi *et al.*, Nivolumab plus ipilimumab or nivolumab alone versus ipilimumab alone in advanced melanoma (CheckMate 067): 4-Year outcomes of a multicentre, randomised, phase 3 trial. *Lancet Oncol.* **19**, 1480–1492 (2018).
27. M. Obeid *et al.*, Calreticulin exposure dictates the immunogenicity of cancer cell death. *Nat. Med.* **13**, 54–61 (2007).
28. T. Panaretakis *et al.*, Mechanisms of pre-apoptotic calreticulin exposure in immunogenic cell death. *EMBO J.* **28**, 578–590 (2009).
29. C. Pozzi *et al.*, The EGFR-specific antibody cetuximab combined with chemotherapy triggers immunogenic cell death. *Nat. Med.* **22**, 624–631 (2016).
30. R. M. Steinman, Decisions about dendritic cells: Past, present, and future. *Annu. Rev. Immunol.* **30**, 1–22 (2012).
31. M. Feng *et al.*, Phagocytosis checkpoints as new targets for cancer immunotherapy. *Nat. Rev. Cancer* **19**, 568–586 (2019).
32. S. C. Wright *et al.*, Apoptosis and DNA fragmentation precede TNF-induced cytolysis in U937 cells. *J. Cell. Biochem.* **48**, 344–355 (1992).
33. C. C. Chen *et al.*, Cytotoxicity of TNFα is regulated by integrin-mediated matrix signaling. *EMBO J.* **26**, 1257–1267 (2007).
34. R. S. Bystry, V. Aluvihare, K. A. Welch, M. Kallikourdis, A. G. Betz, B cells and professional APCs recruit regulatory T cells via CCL4. *Nat. Immunol.* **2**, 1126–1132 (2001).
35. C. L. Chiang *et al.*, Day-4 myeloid dendritic cells pulsed with whole tumor lysate are highly immunogenic and elicit potent anti-tumor responses. *PLoS One* **6**, e28732 (2011).
36. H. H. Oberg, D. Wesch, S. Kalyan, D. Kabelitz, Regulatory interactions between neutrophils, tumor cells and T cells. *Front. Immunol.* **10**, 1690 (2019).
37. J. Van Loenhout *et al.*, Cold atmospheric plasma-treated PBS eliminates immunosuppressive pancreatic stellate cells and induces immunogenic cell death of pancreatic cancer cells. *Cancers (Basel)* **11**, 1597 (2019).
38. S. Tomić *et al.*, Plasma-activated medium potentiates the immunogenicity of tumor cell lysates for dendritic cell-based cancer vaccines. *Cancers (Basel)* **13**, 1626 (2021).
39. S. Bekeschus *et al.*, xCT (SLC7A11) expression confers intrinsic resistance to physical plasma treatment in tumor cells. *Redox Biol.* **30**, 101423 (2020).
40. S. Bekeschus *et al.*, Cell cycle-related genes associate with sensitivity to hydrogen peroxide-induced toxicity. *Redox Biol.* **50**, 102234 (2022).
41. C. Hetz, The unfolded protein response: Controlling cell fate decisions under ER stress and beyond. *Nat. Rev. Mol. Cell Biol.* **13**, 89–102 (2012).
42. S. Demirsoy, S. Martin, H. Maes, P. Agostinis, Adapt, recycle, and move on: Proteostasis and trafficking mechanisms in melanoma. *Front. Oncol.* **6**, 240 (2016).
43. M. Corazzari, M. Gagliardi, G. M. Fimia, M. Piacentini, Endoplasmic reticulum stress, unfolded protein response, and cancer cell fate. *Front. Oncol.* **7**, 78 (2017).
44. N. Rufo, A. D. Garg, P. Agostinis, The unfolded protein response in immunogenic cell death and cancer immunotherapy. *Trends Cancer* **3**, 643–658 (2017).
45. S. B. Cullinan, J. A. Diehl, PERK-dependent activation of Nrf2 contributes to redox homeostasis and cell survival following endoplasmic reticulum stress. *J. Biol. Chem.* **279**, 20108–20117 (2004).
46. Y. J. Chern *et al.*, The interaction between SPARC and GRP78 interferes with ER stress signaling and potentiates apoptosis via PERK/eIF2α and IRE1α/XBP-1 in colorectal cancer. *Cell Death Dis.* **10**, 504 (2019).
47. L. Galluzzi *et al.*, Consensus guidelines for the definition, detection and interpretation of immunogenic cell death. *J. Immunother. Cancer* **8**, e000337 (2020).
48. K. Wende, S. Reuter, T. von Woedtke, K. D. Weltmann, K. Masur, Redox-based assay for assessment of biological impact of plasma treatment. *Plasma Process. Polym.* **11**, 655–663 (2014).
49. T. Adachi *et al.*, Plasma-activated medium induces A549 cell injury via a spiral apoptotic cascade involving the mitochondrial-nuclear network. *Free Radic. Biol. Med.* **79**, 28–44 (2015).
50. S. Bekeschus *et al.*, Cold physical plasma-treated buffered saline solution as effective agent against pancreatic cancer cells. *Anticancer Agents Med. Chem.* **18**, 824–831 (2018).
51. J. Vaquero *et al.*, Cold-atmospheric plasma induces tumor cell death in preclinical in vivo and in vitro models of human cholangiocarcinoma. *Cancers (Basel)* **12**, 1280 (2020).
52. K. R. Liedtke *et al.*, Non-thermal plasma-treated solution demonstrates antitumor activity against pancreatic cancer cells in vitro and in vivo. *Sci. Rep.* **7**, 8319 (2017).

53. S. Y. Kim, H. J. Kim, H. J. Kim, C. H. Kim, Non-thermal plasma induces antileukemic effect through mTOR ubiquitination. *Cells* **9**, 595 (2020).
54. E. Freund *et al.*, Identification of two kinase inhibitors with synergistic toxicity with low-dose hydrogen peroxide in colorectal cancer cells in vitro. *Cancers (Basel)* **12**, 122 (2020).
55. E. de Bree, C. W. Helm, Hyperthermic intraperitoneal chemotherapy in ovarian cancer: Rationale and clinical data. *Expert Rev. Anticancer Ther.* **12**, 895–911 (2012).
56. H. Tanaka *et al.*, Non-thermal atmospheric pressure plasma activates lactate in Ringer's solution for anti-tumor effects. *Sci. Rep.* **6**, 36282 (2016).
57. G. Bruno *et al.*, Cold physical plasma-induced oxidation of cysteine yields reactive sulfur species (RSS). *Clin. Plas. Med.* **14**, 100083 (2019).
58. J. W. Lackmann *et al.*, Nitrosylation vs. oxidation – How to modulate cold physical plasmas for biological applications. *PLoS One* **14**, e0216606 (2019).
59. S. Wenske *et al.*, Nonenzymatic post-translational modifications in peptides by cold plasma-derived reactive oxygen and nitrogen species. *Biointerphases* **15**, 061008 (2020).
60. S. Wenske *et al.*, Reactive species driven oxidative modifications of peptides-tracing physical plasma liquid chemistry. *J. Appl. Phys.* **129**, 193305 (2021).